

The Electrochemical Behavior of Au/AuNPs/PNA/ZnSe-QD/ACA Electrode Towards CySH Oxidation

Azadeh Azadbakht · Amir Reza Abbasi · Zohreh Derikvand · Ziba Karimi

Received: 14 September 2014 / Accepted: 5 December 2014 / Published online: 30 January 2015
© The Author(s) 2015. This article is published with open access at Springerlink.com

Abstract This work describes the electrochemical behavior of azodicarboxamide (ACA) film immobilized on the surface of penicillamine (PNA)/ZnSe-quantum dot (ZnSe-QD) gold nanoparticle (AuNPs) Au electrode. Electrocatalytic activity of modified electrode toward the oxidation of cysteine (CySH) was investigated. The surface structure and composition of the sensor were characterized by scanning electron microscopy (SEM). Oxidation of CySH on the surface of modified electrode was investigated with cyclic voltammetry, electrochemical impedance spectroscopy (EIS), hydrodynamic voltammetry and chronoamperometry methods. The results show that the PNA/ZnSe-QD/ACA film displays excellent electrochemical catalytic activities towards CySH oxidation. The modified electrode shows reproducible behavior and high level of stability during the electrochemical experiments. Also it has short response time, low detection limit, high sensitivity and low operation potential, which can be used as an amperometric sensor for monitoring of CySH. The proposed modified electrode was successfully used for determination of CySH in real sample such as human serum.

Keywords Penicillamine (PNA) · Azodicarboxamide (ACA) · ZnSe quantum dot · Electrocatalytic oxidation · Cysteine (CySH)

1 Introduction

Detection of biomolecules at low concentrations is critically important to the early diagnosis and successful treatment of diseases [1–3]. In addition, there have been continuous researches for fabrication of new electrode materials for developing new sensitive and selective electrochemical biosensors for the detection of the trace amounts of biomolecules [1–3]. Sulfur-containing amino acids, such as homocysteine (HCySH) and L-cysteine (CySH) play crucial roles in biological systems for the diagnosis of disease states [4, 5]. CySH is known as an active site in the catalytic function of certain enzymes called CySH proteases and its deficiency is involved in

slowed growth, hair depigmentation, edema, lethargy, liver damage, muscle and fat loss, skin lesions, and weakness. It is also widely used in the food industry as an antioxidant and in the pharmaceutical industry in drug formulation [6–12]. Therefore, the rapid, sensitive and selective detection of CysH are very important for investigating their functions in cells and disease diagnosis [13, 14].

Numerous methods have been reported for the determination of thiols. Most of them are based on the chromatographic separation [15, 16], electrophoretic methods [17, 18] and UV/vis absorption spectrometry [14, 19, 20]. Separation methods present basic limitations in terms of equipment cost, complexity, sample processing and run times. Among different methodologies used, electrochemical measurements of thiols have attracted considerable interest because of their high sensitivity, simplicity, low cost and feasibility to the development in vivo sensors and chromatographic detectors [21, 22]. Various chemically modified electrodes (CMEs) with electrocatalytic

A. Azadbakht (✉) · A. R. Abbasi · Z. Derikvand · Z. Karimi
Department of Chemistry, Faculty of Science, Khorramabad
Branch, Islamic Azad University, Khorramabad, Iran
e-mail: azadbakht.a@gmail.com

properties have been fabricated and applied in the detection of CySH [23–26]. The reported CMEs have their advantages and limitations in linear dynamic range, selectivity, sensitivity, detection limit and other characteristics. As a result, it is necessary to have further efforts to fabricate simple, low cost, stable, sensitive and selective CMEs that can improve the characteristics of electrocatalytic activity for determination of CySH.

By using nanomaterials, some of the aforementioned problems such as instability and sensitivity might be overcome. Quantum dots (QDs) are semiconductor nanocrystals that range from 2 to 10 nm in size. They possess size tunable optical and electronic properties. Their quantum size effects give rise to excellent electrical, optical and electrochemical properties, such as change of electrochemical potential of band edge [27]. Quantum dots have found potential applications in several areas, including catalysis, coatings, textiles, data storage, biotechnology, health care, biomedical, pharmaceutical industries, and most recently in bioanalytical chemistry [28]. When suitably functionalized with amphiphilic bifunctional molecules such as mercapto- carboxylic acids [HS-(CH₂)_n-COOH, *n* = 1–15] [29], the small sizes of quantum dots can allow for rapid transfer of electrons to the surface of the target particles, resulting to a higher charge detaching efficiency [27]. The carboxylic group also offers a convenient surface since it can react favorably with amino group of other compounds. Short chained capping agents such as mercaptopropionic acid (MPA) and CySH have been used for self-assembly on gold electrode [30] and are associated with enhanced electrochemical signals of the quantum dots towards target analytes [31]. Azodicarboxamides (R₂-NCON = NCONR₂) are shown to act as new templates for the assembly of unprecedented azo-functionalized hydrogen-bond-assembled [32].

In this work, we describe an electrochemical method based on azodicarboxamide (ACA) film immobilized on the surface of PNA/ZnSe-quantum dot (ZnSe-QD) gold nanoparticle (AuNPs) Au electrode for detection of CySH. The quantum dot modifier was used to create a nanostructured/nanoscaled platform and 3-mercaptopropionic acid (3MPA) was used as the stabilizing agent to prevent the chalcogenide ZnSe nanocrystals from aggregating. In addition, the carboxylic acid groups of 3MPA can be used for covalent attachment of ACA via *N*-hydroxysuccinimide (NHS) and 1-ethyl-3-(3-dimethylaminopropyl) carbodiimide hydrochloride (EDC) as the condensation agent. From Faraday law, current is directly proportional to the amount of the material undergoing an electrochemical reaction. These translate to changes in the rate of electron transfer or kinetics of an electrochemical reaction.

2 Experimental

2.1 Chemicals

CySH, PNA, *N*-hydroxysuccinimide (NHS), 1-ethyl-3-(3-dimethylaminopropyl) carbodiimide hydrochloride (EDC), 3-mercaptopropionic acid (3MPA), sodium hydroxide, selenium powder, zinc nitrate, sodium citrate and H₂AuCl₄ were purchased from Sigma-Aldrich (St. Louis, USA) and used as received. Sodium citrate, ammonia (25 %), DMSO (99 %) and hydrochloric acid (37 %) were purchased from Merck Company (Germany) and Fluka. All other chemicals were of analytical-reagent grade and used without further purification. Double distilled water was used thoroughly. All experiments were carried out at ambient temperature of 25 ± 1 °C.

2.2 Apparatus

Electrochemical experiments were performed via using a μ Autolab III (Eco Chemie B.V.) potentiostat/galvanostat by NOVA 1.8 software. A conventional three-electrode cell was used with an Ag|AgCl electrode (KCl 3 M) as the reference electrode, a Pt wire as counter electrode and a modified Au as working electrode. The cell was a one-compartment cell with an internal volume of 10 mL. JENWAY pH-meter (model 3345) was also applied for pH measurements. To obtain information about the morphology and size of the particles, scanning electron microscopy (SEM) was performed using an X-30 Philips instrument.

2.3 Synthesis of Gold Nanoparticle

In this study, colloidal AuNPs were prepared in accordance with the literature published before [33]. Then, 0.5 mL of 1 % (w/v) sodium citrate solution was added to 50 mL of 0.01 % (w/v) of H₂AuCl₄ boiling solution. H₂AuCl₄ and sodium citrate aqueous solutions were filtered through a 0.22 μ m microporous membrane filter before use. In this procedure, all glass wares used were cleaned in freshly prepared HNO₃/HCl (1:3) solution and then rinsed thoroughly with doubly distilled water. The mixture was boiled for 15 min and then stirred for 15 min after removing the heating source to produce colloidal AuNPs. The solution was stored in a refrigerator in a dark-colored glass bottle before to use. The synthesized colloidal AuNP shows maximum absorbance intensity in UV-Vis spectra at 520 nm. If such tiny particles are allowed to coalesce, their color can be systematically varied from ruby red through violet to blue. In the current work, colloidal AuNPs were stable for 10 days and their colors remained approximately constant.

2.4 Synthesis of 3-Mercaptopropionic Acid Capped ZnSe Quantum Dots

3MPA-ZnSe quantum dots were prepared according to method described by Andrade et al. [34] with some modification. Solution A (selenide ions) was prepared by mixing 0.16 g of Se powder with 0.15 g of NaBH_4 in a round bottomed flask and adding deionized water to make 100 mL solution, resulting to 0.02 and 0.04 M of Se and NaBH_4 respectively. The mixture was then stirred continuously at room temperature under nitrogen saturation for 25 min, after which a dark yellow solution was formed. Solution B (0.01 M zinc ions) was prepared by dissolving 0.30 g of zinc nitrate hexahydrate in deionized water. Then 100 mL solution 0.696 μL of 3-mercaptopropionic acid (3MPA) was added to the zinc nitrate solution, to make 0.04 M of the capping agent in the final reaction volume (200 mL). The pH of the resulting solution (solution B) was adjusted using NaOH and saturated with nitrogen gas for 30 min. One hundred milliliter of the freshly prepared solution A was added drop wise into the nitrogen saturated solution B. After 40 min, a pale yellow solution was formed. The reaction was then quenched by immediately moving the reaction flask into a freezer at $-20\text{ }^\circ\text{C}$ after the 40 min.

2.5 Electrode Modification

Cysteine has been used to immobilize AuNPs on a bulk gold electrode [33]. The working electrode was an Au disk electrode with a diameter of 3 mm. Prior to each treatment, the Au working electrode (Metrohm) was polished with alumina slurry down to 0.05 μm on a polishing cloth followed by sonication in distilled water and absolute ethanol. Then the Au electrode was electrochemically cleaned by cycling the electrode potential between -0.4 and 1.2 V versus Ag|AgCl electrode in $0.5\text{ M H}_2\text{SO}_4$ at a scan rate of 100 mV s^{-1} until the cyclic voltammetry characteristics for a clean Au electrode were obtained. Then the clean gold electrode was immersed in aqueous solution containing 0.1 M CySH for 2 h at room temperature and darkness. Upon removal from the deposition solution, the substrate was thoroughly rinsed and soaked in distilled water for 12 h to remove the physically adsorbed CySH from the electrode surface. After that, it was dipped into AuNPs colloidal solution for 24 h, in order to immobilize the AuNPs on the modified surface separately and behave as nanoelectrode array. The resultant electrode was washed with water and used for electrochemical measurements (labeled as Au/AuNPs). The Au/AuNPs electrode was immersed in the solution containing 0.1 M PNA for 2 h at room temperature and darkness (Au/AuNPs/PNA). Then the Au/AuNPs/PNA modified electrode was immersed into solution containing ZnSe-QDs (pH 7.4) in presence of

0.1 M EDC for 5 h to form Au/AuNPs/PNA/ZnSe-QD electrode. The resulting quantum dot modified gold electrode was allowed to dry under nitrogen gas. For ACA immobilization, Au/AuNPs/PNA/ZnSe-QD electrode was incubated for 3 h in a 0.1 M phosphate buffer solution (PBS, pH 6.0) containing 0.5 mg mL^{-1} solution of ACA in presence of 0.1 M EDC and NHS at $4\text{ }^\circ\text{C}$ (the electrode denoted as Au/AuNPs/PNA/ZnSe-QD/ACA). ACA was immobilized on the Au/AuNPs/PNA/ZnSe-QD modified electrode surface by the amide bond formation between the activated EDC and NHS treated carboxylic acid groups of the film and the amine groups on the ACA as demonstrated in Scheme 1.

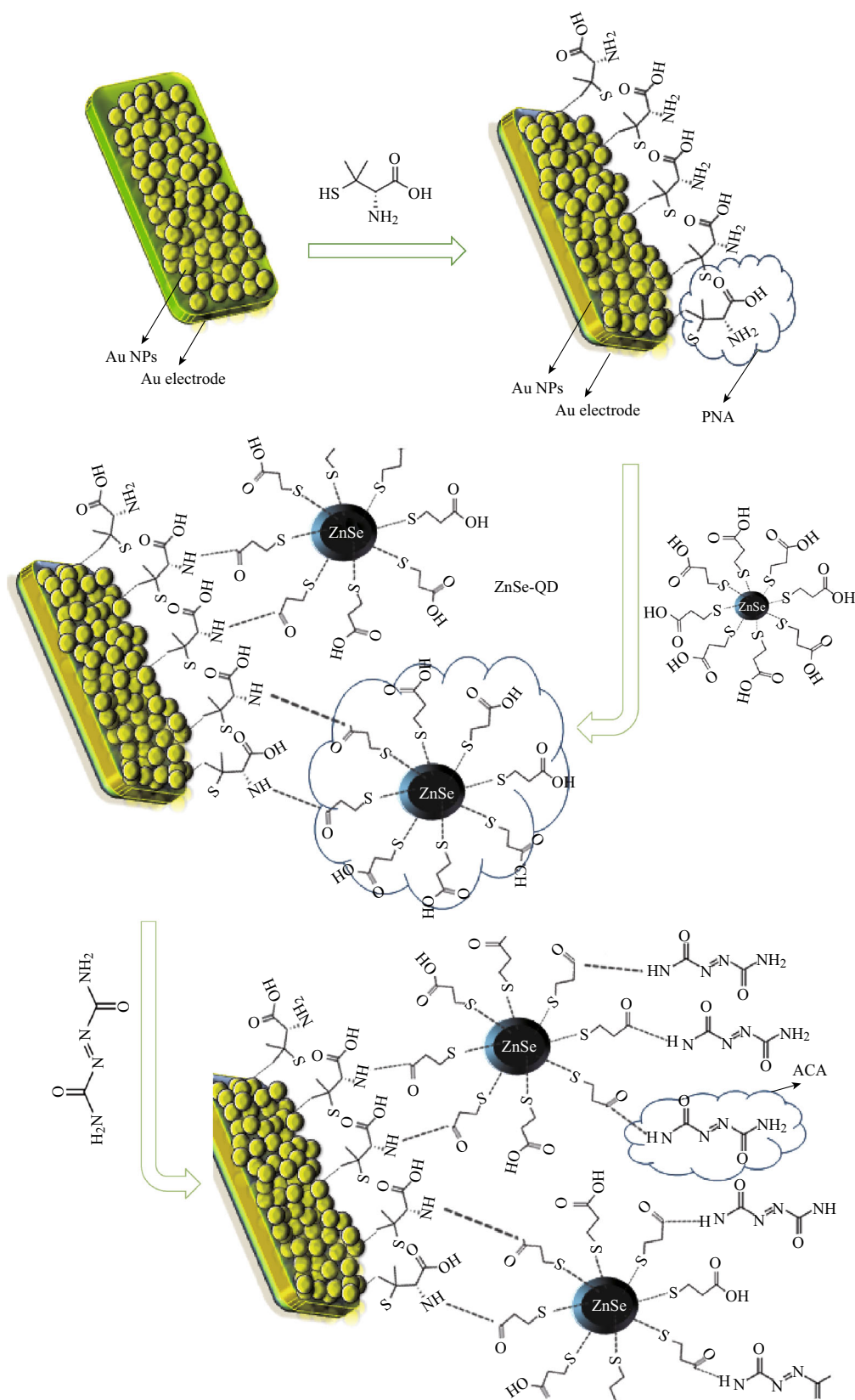
For comparison, the modification of Au/AuNPs/PNA/ZnSe-QD with ACA was also carried out by electrodeposition of ACA at the surface of electrode. For this purpose, ACA was immobilized at the surface of modified electrode by immersion Au/AuNPs/PNA/ZnSe-QD in solution containing 0.5 mg mL^{-1} ACA. Then the electrode potential was cycled between -0.3 and 0.3 V at a scan rate of 50 mV s^{-1} for 50 cycles. The result indicated that there is a considerable enhancement in the charge of voltammogram when the electrode position of ACA at the surface of Au/AuNPs/PNA/ZnSe-QD was occurred compared with the amide bond formation in the first case. This behavior may be attributed to saturation of active site of 3-mercaptopropionic acid in the film with the amide bond formation between the carboxylic acid groups of the 3MPA acid and the amine groups on the ACA.

To investigate the role of AuNPs, the modification of Au electrode was also carried out by immersion of gold electrode directly in the solution containing 0.1 M PNA and then ZnSe-QD in presence of 0.1 M EDC to form Au/PNA/ZnSe-QD electrode. Furthermore, the role of ZnSe-QD investigation was carried out by immersion of Au electrode in the solution containing 0.1 M CySH for 2 h and then into AuNPs colloidal solution for 24 h. At last, the surface of Au/PNA/ZnSe-QD and Au/AuNPs were modified by electrode position of ACA on the surface using the foregoing procedure (the electrodes denoted as Au/PNA/ZnSe-QD/ACA and Au/AuNPs/ACA). The other used electrode (Au/ACA) was prepared by electrode position of ACA on the surface of bare Au electrode as described above.

3 Results and Discussion

3.1 Characterization of the Au/AuNPs/PNA/ZnSe-QD/ACA Electrode by SEM

To investigate the surface structure and morphology of the modified electrode, we performed SEM. Figure 1 shows the SEM images of bare Au (Fig. 1a) and other modified electrodes. The formation of AuNPs layer on the electrode



Scheme 1 Overall preparative process of the Au/AuNPs/PNA/ZnSe-QD/ACA electrode

surface testified by SEM is shown in Fig. 1b. It can be seen that a uniform film of AuNPs immobilized onto the electrode surface. The SEM image of Au/AuNPs/PNA/ZnSe-QD modified electrode is shown in Fig. 1c in which the morphology of the electrode surface is obviously changed by the amide bond formation between the activated EDC and NHS treated carboxylic acid groups on the 3MPA/ZnSe-QD and the amine groups of the film (PNA) [35]. Figure 1d provides the SEM image of Au/AuNPs/PNA/ZnSe-QD/ACA electrode. As can be seen the generated ACA nanoparticles were homogenously distributed in the matrix of ZnSe-QD. The results indicate that the film has a globular structure with relatively homogeneous distribution. The presence of smaller nanoparticles leads to an increase in the surface coverage for adsorption of more CySH. This structure indicates that CySH can penetrate through the deposit and access the underlying layer, and therefore it can be fully utilized.

3.2 Electrochemical Behavior of Au/AuNPs/PNA/ZnSe-QD/ACA Electrode

The cyclic voltammograms of the ACA immobilized at the surface of Au, Au/AuNPs, Au/AuNPs/PNA and Au/AuNPs/PNA/ZnSe-QD in 0.1 M PBS (pH 6.0) at a scan rate of 50 mV s^{-1} was examined. As can be seen in Fig. 2, a pair of ill redox peaks were observed when Au/ACA (curve a) was used. Comparison of these results with that obtained with Au/AuNPs/ACA (curve c) reveals the role of AuNPs as the underlying film, which increases the peak current. This may be due to increasing the surface area of the electrode. Modification of the Au/AuNPs electrode with PNA (Au/AuNPs/PNA/ACA) decreases the electrode response (curve b) and shifted the redox peak potentials towards positive values. This may be attributed to the increase of path length of electron transfer between redox center and the surface of the bare electrode. Despite this, presences of the PNA in the modified electrode not only stabilize the QD nanoparticle, but also have the advantages of very uniform distribution of nanometer sized particles.

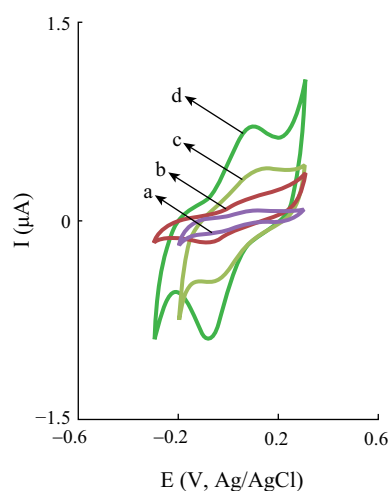


Fig. 2 Cyclic voltammograms of Au/ACA (curve a), Au/AuNPs/PNA/ACA (curve b), Au/AuNPs/ACA (curve c) and Au/AuNPs/PNA/ZnSe-QD/ACA (curve d) in 0.1 M PBS (pH 6.0) at a scan rate of 50 mV s^{-1}

In order to enhance the surface area of the Au/AuNPs/PNA/ACA electrode and its sensitivity for monitoring the analysts, improvement of the mentioned electrode was carried out. For this purpose, ZnSe-QD was used (Au/AuNPs/PNA/ZnSe-QD/ACA) and its CV was recorded and compared with those obtained with other tested electrodes (curve d). As it is seen from Fig. 2, the electrode improves the reversibility of the electrodic process (peaks potential separation was decreased to 110 mV ($E_{pa} = 0.052$ and $E_{pc} = -0.058$)). Also, its peak currents increase 2 times higher than that obtained with the Au/AuNPs/PNA/ACA electrode. The generated ZnSe-QD was homogenously distributed along the PNA, constructing individual elements of the electrode [36].

Electrochemical impedance spectroscopy (EIS) technique has been proved to be an effective method for probing the features of surface modified electrodes. Figure 3 shows the typical Nyquist plots for bare Au, Au/AuNPs, Au/AuNPs/PNA, Au/AuNPs/PNA/ZnSe-QD and

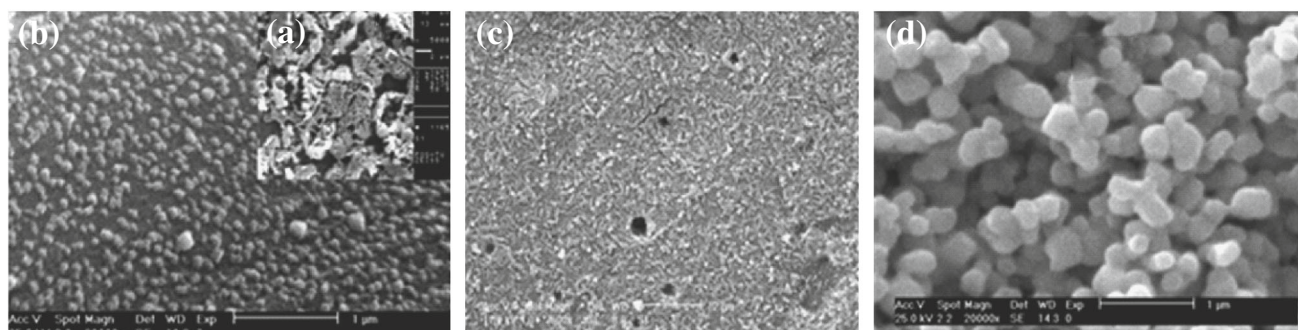


Fig. 1 Typical SEM images of various electrodes: a bare Au bare, b Au/AuNPs, c Au/AuNPs/PNA/ZnSe-QD, and d Au/AuNPs/PNA/ZnSe-QD/ACA

Au/AuNPs/PNA/ZnSe-QD/ACA electrodes recorded in 0.1 M KCl solution containing 0.5 mM $\text{Fe}(\text{CN})_6^{3-/4-}$ as an electrochemical redox marker. The straight line at low frequency is related to the diffusion process known as Warburg element, while the high frequency semicircle is related to R_{et} which controls the electron transfer kinetics of the redox probe at the electrode interface [13]. The EIS at a bare Au electrode displays a very small semicircle and the charge transfer resistance, which was a characteristic feature of the diffusion controlled electrochemical processes (Fig. 3a). After modification of Au electrode with AuNPs, R_{et} decreased and it can be seen that an almost straight line is exhibited. This behavior proved that the assembly of AuNPs makes the electron transfer easier (Fig. 3b). After immobilization of PNA, the value of R_{et} is significantly increased to about 520 Ω . It indicates hindrance to the electron transfer, confirming the successful immobilization of PNA onto Au/AuNPs electrode surface (Fig. 3c). Subsequently, when the Au/AuNPs/PNA electrode was modified with ZnSe-QD layer, R_{et} increased to 982 Ω (Fig. 3d), suggesting that the semiconductor film was successfully immobilized on the electrode surface. The observed increase can be attributed to the electrostatic repulsion between $[\text{Fe}(\text{CN})_6]^{3-/4-}$ redox marker and $\text{SCH}_2(\text{CH}_2)\text{COO}^-$ complexes. For the Au/AuNPs/PNA/ZnSe-QD/ACA modified electrode, the R_{et} decreased to 418 Ω , which confirms that the ACA complex have been successfully attached to the electrode surface and makes the electron transfer easier (Fig. 3e). These results indicate that the Au/AuNPs/PNA/ZnSe-QD/ACA electrode could provide good electron conduction pathways between the electrode and electrolyte.

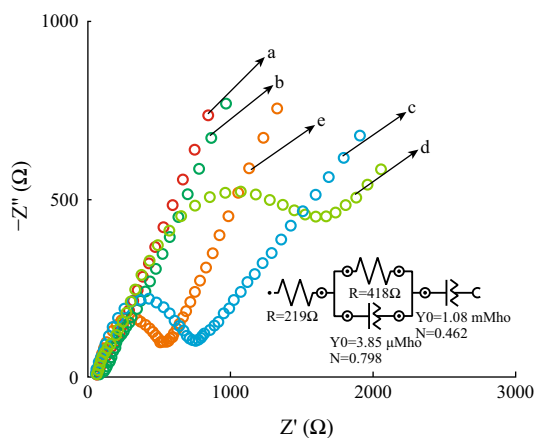


Fig. 3 Nyquist plots for bare Au (curve a), Au/AuNPs (curve b), Au/AuNPs/PNA (curve c), Au/AuNPs/PNA/ZnSe-QD (curve d) and Au/AuNPs/PNA/ZnSe-QD/ACA (curve e) electrodes recorded in 0.1 M KCl solution containing 0.5 mM $\text{Fe}(\text{CN})_6^{3-/4-}$ in the frequency range of 10 kHz–0.1 Hz. Inset the equivalent circuit used to fit the experimental impedance data

3.3 Properties of the Nano-structured Au/AuNPs/PNA/ZnSe-QD/ACA Electrode

In the preliminary experiments the electrochemical behavior of ACA was studied at the surface of Au/AuNPs/PNA/ZnSe-QD electrode using cyclic voltammetric technique. The results showed one pair of redox peaks with a formal potential of 0.03 V versus Ag/AgCl electrode.

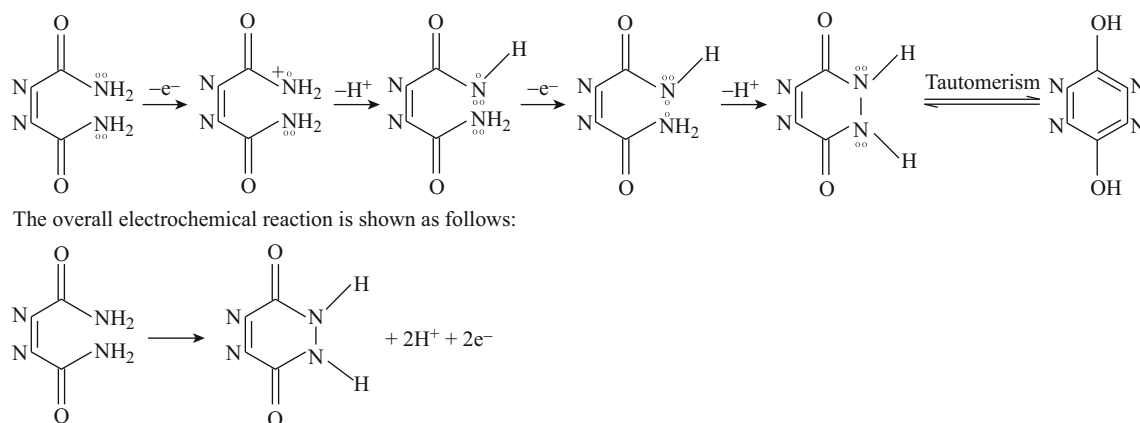
The effect of pH on the electrochemical behavior of ACA at the surface of Au/AuNPs/PNA/ZnSe-QD electrode was also studied at pH values ranging from 1 to 7. A well-defined redox peaks were observed at acidic media (pH < 7). At pH_s greater than 7, the shape and the reproducibility of redox peak were poor. The results revealed that the maximum peak current was obtained at pH 6. The potential of the anodic peak of ACA was shifted linearly toward less positive potential values with increasing the pH between 1 and 7 by slope of 98 mV pH⁻¹. The number of hydrogen ions participated in the rate determining step (Z_{H^+}) can be obtained from the slope value of the linear segment of the E_p –pH plot ($59Z_{H^+}/(1-\alpha)n$). The slope of 98 mV/pH for ACA oxidation indicating that the number of protons involved in the reaction mechanisms is equal to number of electron precipitate in electrodic process ($Z_{H^+}/n = 98 \times (1-0.41)/59 = 0.98$). (α was calculated from Eq. 2).

Furthermore, effect of the scan rate on the CVs of ACA was studied. From the plot of I_p versus $v^{1/2}$, the number of electrons (n) involved in the overall reaction was obtained according to the following equation [37]:

$$I_p = 2.99 \times 10^5 n(1 - \alpha)^{1/2} A C_b D^{1/2} v^{1/2} \tag{1}$$

where A is electrode surface area, C_b is the ACA concentration and D is the diffusion coefficient (D was calculated from chronoamperometry technique). From the slope of the I_p versus $v^{1/2}$ plot, the total number of electrons (n) is about two. Based on the above results, a possible reaction mechanism of oxidation process is suggested as shown in Scheme 2).

Figure 4a exhibits the recorded cyclic voltammograms of Au/AuNPs/PNA/ZnSe-QD/ACA film in 0.1 M PBS (pH 6) at different scan rates. In Fig. 4b, the plots of anodic and cathodic peak currents versus the scan rate are presented for the modified electrode. As is obvious, both the anodic and cathodic peak currents are linearly proportional to the scan rate in the range of 10–400 mV s⁻¹, ($R^2 = 0.998$ and 0.993 for anodic and cathodic peak, respectively) indicating a surface confined electrode process. The peak-to-peak potential separation is about 100 mV at scan rates below 50 mV s⁻¹, suggesting facile charge transfer kinetics over this range of sweep rates. At higher sweep rates ($v > 100$ mV s⁻¹) peak separations begin to increase,



Scheme 2 Suggested mechanism for the redox peak of ACA

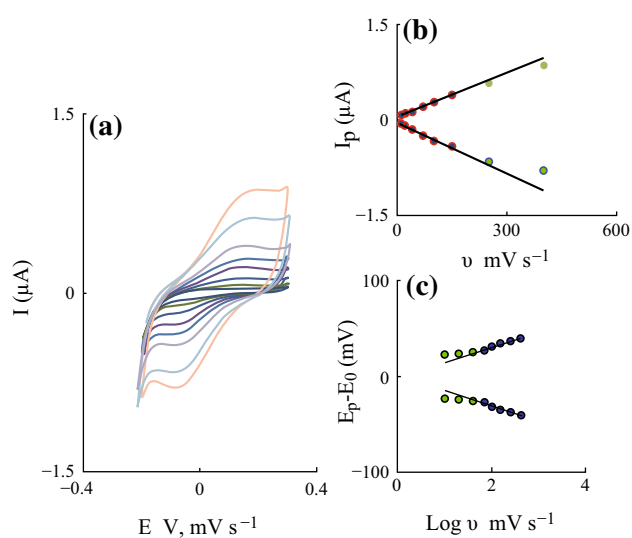


Fig. 4 **a** Cyclic voltammetric response of Au/AuNPs/PNA/ZnSe-QD/ACA modified electrode in 0.1 M PBS (pH 6.0) at different scan rates; from inner to outer: 10, 20, 40, 70, 100, 150, 250, and 400 mV s^{-1} . **b** Plot of peak currents vs. scan rate. **c** Plot of $(E_p - E_0)$ (mV) versus $\log v$

indicating the limitation due to charge transfer kinetics. The shifts of peak potentials were proportional to the logarithm of the scan rate for scan rates higher than 100 mV s^{-1} ($R^2 = 0.989$ and 0.988 for anodic and cathodic peak, respectively) (see Fig. 4c).

Based on Laviron theory [38], the electron transfer rate constant (k_s) and charge transfer coefficient (α) can be determined. By measuring the variation of peak potential with scan rate, using the following Eq. 1, the charge transfer coefficient (α) was determined:

$$E_p = K_s - 2.3030 (RT/\alpha nF) \log v \quad (2)$$

The slope of ΔE_{pc} versus $\log v$ was about 50 mV and the electrons transferred for ACA were 2 (from Eq. 1), and then α were calculated as 0.41. By introducing α value in

the following Eq. 3, for $\Delta E_p \geq 200/n$ mV, the electron transfer rate constant was estimated to be $0.31 \pm 0.03 \text{ s}^{-1}$.

$$\text{Log} k_s = \alpha \log(1 - \alpha) + (1 - \alpha) \log \alpha - \log(RT/nFv) - \alpha \log(1 - \alpha) nF \Delta E_p / 2.3RT \quad (3)$$

The large value obtained for k_s indicates high ability of ZnSe-QD nanoparticles for promoting the transfer of electrons between ACA and the electrode surface. The surface coverage concentration (Γ) of ACA was estimated by integrating the area under the cathodic peak. According to the equation $Q = \Gamma/nFA$ and assuming $A = 0.12 \text{ cm}^2$, the surface concentration of the proposed molecule was about $1.46(\pm 0.20) \times 10^{-8} \text{ mol cm}^{-2}$. The surface concentration value indicated the formation of multilayer of ACA on the Au/AuNPs/PNA/ZnSe-QD modified electrode and high loading ability of ZnSe-QD nanoparticles for immobilization of ACA [39].

The long term stability of the Au/AuNPs/PNA/ZnSe-QD/ACA modified electrode and the reversibility of its electrochemical behavior were also investigated. It was found that after storing the electrode in ambient condition for 1 week, the current and potential response of recorded cyclic voltammograms remained almost unchanged. In addition, the operational stability of the modified electrode was examined by recording of the repetitive cyclic voltammograms in 0.1 M PBS (Fig. 5). The results indicated that after 100 repetitive cycles at a scan rate of 50 mV s^{-1} , no detectable change was observed at the peak height and potential separation. The high stability of Au/AuNPs/PNA/ZnSe-QD/ACA modified electrode may be related to the mechanical and chemical stability of ZnSe-QD film along with the attachment of ACA. This behavior leads to its stabilizing against desorption and avoids it from leaching into the solution. In order to study the reproducibility of the electrode modification, five Au/AuNPs/PNA/ZnSe-QD/ACA modified electrodes were prepared independently. For five successive prepared electrodes, the relative

standard deviation (RSD) of measuring anodic peak currents was only 5 %.

3.4 Electrocatalytic Oxidation of CySH at Au/AuNPs/PNA/ZnSe-QD/ACA Electrode

Application of the modified electrode for oxidation of CySH was evaluated by cyclic voltammetry. Oxidation of CySH at Au/AuNPs/PNA/ZnSe-QD electrode and Au/AuNPs/PNA/ZnSe-QD/ACA electrodes were investigated in 0.1 M PBS (pH 6.0). Figure 6 shows recorded cyclic voltammograms in the absence and presence of 2 mM CySH at Au/AuNPs/PNA/ZnSe-QD and Au/AuNPs/PNA/ZnSe-QD/ACA electrodes with scan rate of 50 mV s^{-1} . As can be seen, no electrochemical response at Au/AuNPs/PNA/ZnSe-QD electrode was observed in the absence of CySH (voltammogram “c”), but in the presence of CySH a small redox response can be seen (voltammogram “d”). However, in the same conditions at Au/AuNPs/PNA/ZnSe-QD/ACA electrode, the oxidation current of CySH starts at -0.15 V and an obvious catalytic oxidation peak appears at the potential of 0.05 V (voltammogram “b”). It can be seen that peak potential for oxidation of CySH is significantly shifted to a more negative potential (0.05 V vs. Ag|AgCl) compared with Au/AuNPs/PNA/ZnSe-QD modified electrode (0.55 V vs. Ag|AgCl). Furthermore, the anodic peak current was greatly enhanced in the presence of CySH and the reduction peak current totally disappeared, suggesting a typical electrocatalytic oxidation process. The substantially decreasing overvoltage and increasing oxidation peak current of CySH confirm that ACA immobilized onto Au/AuNPs/PNA/ZnSe-QD electrode can act as an efficient mediator to shuttle electrons between CySH and working electrode.

To understand the undergoing electrochemical reactions at the different modified electrodes, the EIS experiments

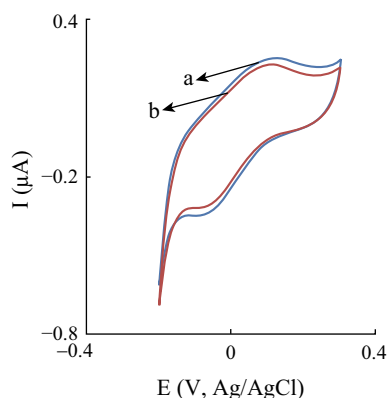


Fig. 5 The first (a) and 100th (b) cyclic voltammograms of Au/AuNPs/PNA/ZnSe-QD/ACA modified electrode in 0.1 M PBS (pH 6.0) at scan rate of 50 mV s^{-1}

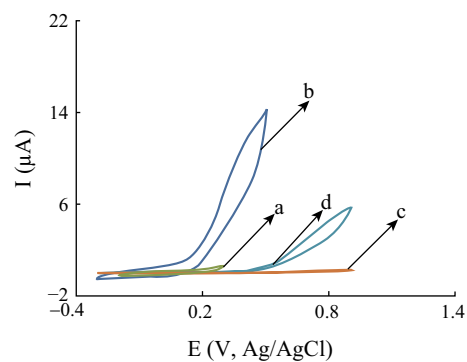


Fig. 6 Cyclic voltammograms of Au/AuNPs/PNA/ZnSe-QD/ACA (curves a and b) and Au/AuNPs/PNA/ZnSe-QD (curves c and d) electrodes in the absence (curves a and c) and presence (curves b and d) of 2 mM of CySH in 0.1 M PBS (pH 6.0) at scan rate of 50 mV s^{-1}

were performed in the presence of 4 mM of CySH in 0.1 M PBS (pH 6.0). As can be seen in Fig. 7 for Au electrode, a semicircle curve was observed over the whole frequency region and the value of R_{et} is $1,100 \Omega$, indicating that the reaction is kinetically controlled (Fig. 7a). After immobilization of ACA at the surface of gold electrode, the value of R_{et} was significantly decreased to about 120Ω (Fig. 7b). These results indicate that the immobilized ACA increases the charge transfer kinetics to about one-ninth of that at the bare Au electrode. It also confirmed that presence of ACA film on Au electrode had a catalytic effect for oxidation of CySH. For Au/PNA/ZnSe-QD/ACA (Fig. 7c) and Au/AuNPs/PNA/ZnSe-QD/ACA (Fig. 7d) the calculated charge transfer resistance are decreased, which proves that the assembly of AuNPs nanoparticles and ZnSe-QD makes the electron transfer easier. The deposition of AuNPs and ZnSe-QD on the surface of modified electrode facilitates the electron transfer of the electrochemical probe on the modified electrode.

For further investigation of the electrocatalytic properties of different modified electrodes, cyclic voltammograms of these electrodes in the presence of CySH at a wide potential range were recorded. The cyclic voltammetric responses of Au/AuNPs/PNA/ZnSe-QD/ACA, Au/AuNPs/ACA, Au/PNA/ZnSe-QD/ACA, Au/ACA, and Au/AuNPs electrodes in 0.1 M PBS in the absence and presence of 5 mM CySH were recorded. CySH did not undergo oxidation at Au/AuNPs electrode in the potential window of -0.4 – 0.4 V in 0.1 M PBS and a pair of ill redox peaks were observed when Au/ACA was used. However, presence of ACA film on Au/AuNPs electrode had a catalytic effect for oxidation of CySH. The result shows that in the absence of CySH a pair of redox peaks corresponding to the $(ACA)_{ox}/(ACA)_R$ couple were observed at the surface of the electrodes tested. Upon addition of CySH, an enhancement in the anodic peak

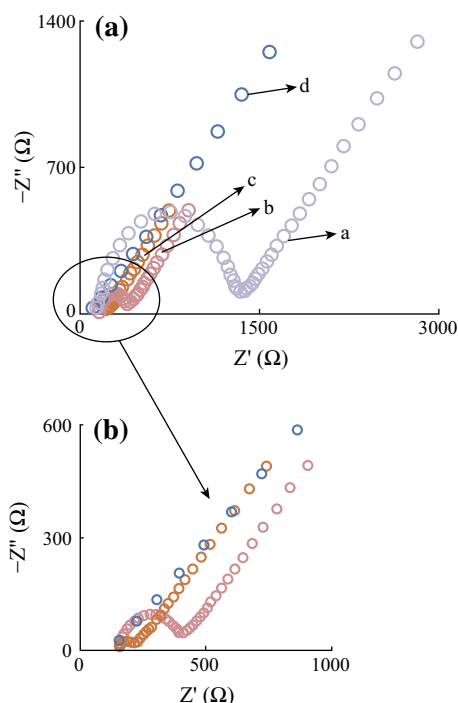


Fig. 7 Nyquist plots of bare Au electrode (curve a), Au/ACA (curve b), Au/PNA/ZnSe-QD/ACA (curve c) and Au/AuNPs/PNA/ZnSe-QD/ACA (curve d) in 0.1 M in PBS containing 4 mM CySH in the frequency range of 10 kHz–0.1 Hz

current was observed and the cathodic peak current tended to decrease. The reason for this increase is that, along with the anodic potential sweep, CySH reduces $(ACA)_{ox}$ to $(ACA)_R$. Simultaneous oxidation of the regenerated $(ACA)_R$ causes an increase in the anodic current. For the same reason, the cathodic current is smaller in the presence of CySH indicating that $(ACA)_{ox}$ is consumed during a chemical step. Moreover, the electrocatalytic oxidation peak current of CySH at Au/AuNPs/PNA/ZnSe-QD/ACA electrode is 12 μA , which is 1.7 times larger than that at Au/AuNPs/ACA electrode (7 μA) and 2.1 times larger than that at Au/PNA/ZnSe-QD/ACA electrode. This behavior is in agreement with EIS data for charge transfer kinetics on the different modified electrodes. These results indicate that presence of ZnSe-QD and AuNPs in the modified electrode supplied a larger surface area to allow more deposition of ACA complex for oxidation of CySH.

Cyclic voltammograms of different concentrations of CySH (ranging from 0.5 to 90 mM) at the modified electrode in 0.1 M PBS were recorded. The calibration curve based on the anodic peak current is linear with the CySH concentration in the range of 0.5–35 mM with a correlation coefficient of 0.996 (Fig. 8b, blue symbols). The response of modified electrode was deviated from the linearity for CySH concentration above 35 mM (Fig. 8b, red symbols). This behavior may be attributed to saturation of some

redox sites on the surface of electrode, which are involved in the catalytic reaction. As can be seen from Fig. 8a–c (magnification at low concentration) by increasing the concentration of CySH, the anodic peak current of the modified electrode is increased while its cathodic peak current decreased, indicating a typical electrocatalytic oxidation process (EC').

For investigation the electrocatalytic mechanism of the modified electrode toward CySH oxidation, cyclic voltammograms of modified electrode in 5 mM CySH containing 0.1 M PBS (pH 6.0) at different scan rates were recorded. Figure 9a illustrates cyclic voltammograms of 5 mM CySH using modified electrode at potential sweep rates ranging from 10 to 150 $mV s^{-1}$.

The anodic peak currents obtained were linear with respect to the square root of the potential sweep rate ($R^2 = 0.997$) (Fig. 9b), which indicates the mass transfer controlled process. Also, it can be seen that the anodic peak potential shifts toward positive potentials by increasing the scan rate. This behavior suggests a kinetic limitation in the reaction between redox sites of the Au/AuNPs/PNA/ZnSe-QD/ACA electrode and CySH. The α value of the electrocatalytic reaction can be evaluated from the following equation [40]:

$$E_p = (b/2)\log v + \text{constants} \quad (4)$$

On the basis of Eq. 4, the slope of E_p versus $\log v$ plot is $b/2$, where b indicates the Tafel slope ($b = 2.3RT/n_\alpha F(1 - \alpha)$). The plot of E_p versus $\log v$ indicates a linear variation for scan rates ranging 10–150 $mV s^{-1}$ (Fig. 9c). The slope is $\partial E_p / \partial \log v$, which was found to be 0.0315 V with correlation coefficient of 0.994. So, $b = 2 \times 0.0315 = 0.063$ V. Assuming that the number of electrons transferred in the rate limiting step is equal to 2, a transfer coefficient of α was estimated as 0.53. Taking into account all these

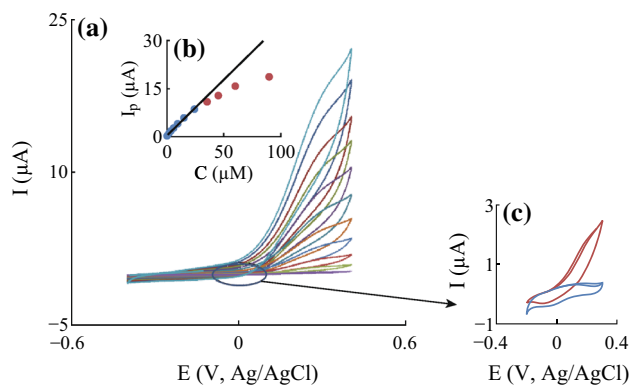


Fig. 8 a CVs of the Au/AuNPs/PNA/ZnSe-QD/ACA in the presence of different CySH concentration: 0.5, 1, 3, 5, 9, 15, 24, 35, 45, 60, and 90 mM respectively in 0.1 M in PBS at a scan rate of 50 $mV s^{-1}$. b Inset the plot of catalytic peak versus CySH concentration, c the detailed magnified region

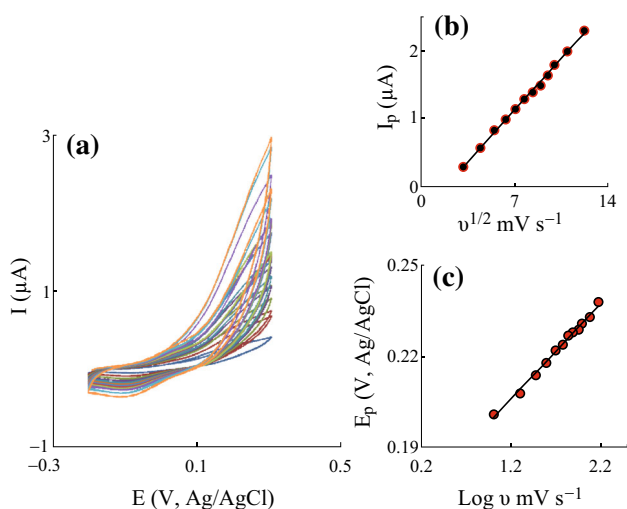
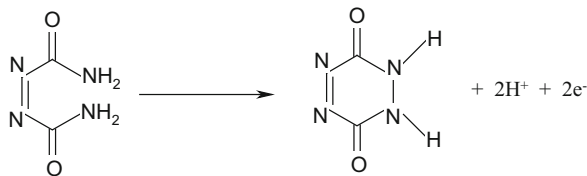
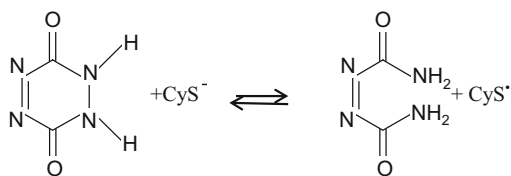


Fig. 9 **a** Cyclic voltammograms of the modified electrode in the presence of 5 mM CySH at various scan rates: 10, 20, 40, 70, 100, 150, 250, and 400 mV s^{-1} in 0.1 M in PBS. **b** Variation of anodic peak currents versus square root of potential scan rate, **c** dependence of the anodic peak potential versus $\log v$

observations, a possible mechanism of CySH electrooxidation on Au/AuNPs/PNA/ZnSe-QD/ACA electrode may be as follows:



(6)



(7)



This is similar to the mechanism reported previously for CySH oxidation on solid electrodes [41]. For CySH oxidation at the surface of Au/AuNPs/PNA/ZnSe-QD (Fig. 6 curve d) a possible mechanism may be as follows [26]:



3.5 Chronoamperometric Studies

The chronoamperometry (CA) method, as well as other electrochemical methods was employed for the investigation of electrode processes at chemically modified electrodes. The result shows a series of well-defined chronoamperograms for the Au/AuNPs/PNA/ZnSe-QD/ACA in the absence and presence of different concentrations of CySH at an applied potential of 0.05 versus Ag/AgCl. For an electroactive material with diffusion coefficient of D , the corresponding current of the electrochemical reaction (under diffusion control) is described by Cottrell's law [39]:

$$I = nFAD^{1/2}C_0\pi^{-1/2}t^{-1/2} \tag{12}$$

where D and C_0 are the diffusion coefficient and bulk concentration, respectively. The average value of D obtained from the slopes of I versus $t^{-1/2}$ plots for different concentrations of CySH is $1.21 \times 10^{-6} \text{ cm}^2 \text{ s}^{-1}$. Chronoamperometry can be used for the evaluation of the catalytic rate constant. At intermediate times, the catalytic current (I_{cat}) is dominated by the rate of electrocatalyzed oxidation of CySH. The rate constant for the chemical reaction between CySH and redox sites was determined according to the method described in the literature [42]:

$$I_{\text{cat}}/I_L = \left[\gamma^{1/2} \left[\pi^{1/2} \text{erf}(\gamma^{1/2}) + \exp(-\gamma)/\gamma^{1/2} \right] \right] \tag{13}$$

where I_{cat} and I_L are the currents of the Au/AuNPs/PNA/ZnSe-QD/ACA electrode in the presence and absence of CySH, and $\gamma = kC_0t$ is the dimensionless kinetic parameter, k is the catalytic rate constant, C_0 is the bulk concentration of CySH, erf is error function and t is the elapsed time. In such cases where $\gamma > 2$, erf ($\gamma^{1/2}$) is almost equal to unity. The above equation can be reduced to:

$$I_{\text{cat}}/I_L = \gamma^{1/2} \pi^{1/2} = \pi^{1/2} (kC_0t)^{1/2} \tag{14}$$

From the slope of the I_{cat}/I_L versus $t^{1/2}$ plot, the average value of k_{cat} was found to $4.25 \times 10^2 \text{ M}^{-1} \text{ s}^{-1}$.

3.6 Amperometric Detection of CySH at the Modified Electrode

Since amperometry under stirred conditions has a much higher current sensitivity than cyclic voltammetry, it was used to estimate the lower limit of detection. Figure 10a shows a typical steady-state catalytic current time response of the rotating modified electrode (2,000 rpm) with successive injection of 1 μM of CySH at an applied potential of 0.05 V versus the reference electrode.

As shown, during the successive addition of CySH a well-defined response was observed, demonstrating stable and efficient catalytic ability of the AuNPs/PNA/ZnSe-QD/

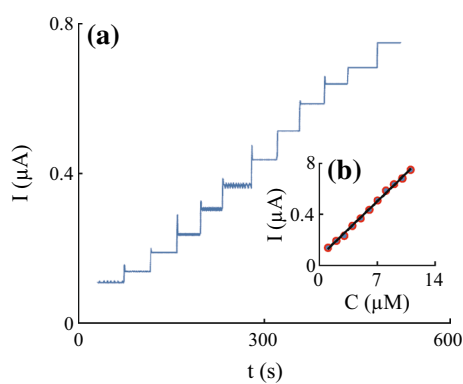


Fig. 10 **a** Amperometric response of rotating sensor during CySH addition (potential = 0.05 V, pH 6, and rotation speed of 2,000 rpm, successive addition of 1 μM CySH). **b** Plots of current versus CySH concentration

ACA film immobilized the surface of electrode. The calibration plot over the concentration range of 1–11 μM (11 points) is linear with a correlation coefficient of 0.9994 and the detection limit of 0.04 μM at the signal to noise ratio of 3. Detection limit and linear calibration range of the proposed method were compared with those obtained in other reports and the results are summarized in Table 1. Although the linear range of the proposed modified electrode is smaller than those reported in some previous works its detection limit is comparable or better than the results reported for CySH determination at the surface of recently fabricated modified electrodes [25, 43–51].

3.7 Application of Electrochemical Sensor for Determination of CySH in Human Serum Samples

To demonstrate the application of the CySH electrochemical sensor, CySH concentrations in real samples were measured. A serum sample of a healthy volunteer was stored frozen

Table 2 Determination of L-cysteine in human serum samples (% \pm RSD calculated & based on five measurements)

Sample	Added (μM)	Found (μM)	Recovery (%)
Serum sample 1	–	205.0 \pm 4.0	
	20.0	224.0 \pm 5.0	99.5 \pm 2.0
	60.0	269.6 \pm 4.0	101.5 \pm 1.5
Serum sample 2	–	200.5 \pm 4.0	
	20.0	222.5 \pm 4.0	100.9 \pm 2.0
	60.0	253.5 \pm 4.5	97.5 \pm 1.5

until assay. 2 mL of methanol was added to 1.5 mL of serum sample. After vortexing the serum sample for 2 min, the precipitated proteins were separated by centrifugation for 3 min at 6,000 rpm. The clear supernatant layer was filtered to obtain protein free human serum sample and its volume was adjusted to 150 mL using double distilled water, then 15 mL of this adjusted solution was tested. Due to interference of ascorbic acid, citric acid, nitrite and uric acid [52, 53], the modified electrode covered with a thin film of nafion is used for CySH detection in real samples. Nafion film is a cation exchange polymer and repels ascorbic acid and other negatively charged species at optimized conditions [54]. The standard addition method was used for simple evaluation of CySH in serum sample. The concentration of CySH in serum sample is found to be 200.5–269.6 μM , which is a normal dosage for CySH in serum samples [55, 56]. Table 2 shows the results obtained for CySH content of the real samples. It is obvious that the obtained recovery rates are in the range of 97.5–101.5 %. Therefore, the modified proposed sensor can be used for CySH detection in real samples.

4 Conclusions

A new composite material modified electrode as Au/AuNPs/PNA/ZnSe-QD/ACA was prepared by

Table 1 Electrochemical response for L-cysteine using various modified electrodes

Electrode	Linear range (μM)	LoD (μM)	Ref.
Electrospun carbon nanofibers modified CPE	0.15–63.8	0.10	[43]
PolyN,Ndimethylaniline/ferrocyanide film/CPE	7.40–138	6.38	[44]
Ordered mesoporous carbon	3.00–130	0.10	[45]
Lead ruthenate pyrochlore modified electrode	Up to 560	1.70	[46]
Cobalt(II) salophen-modified CPE	2.00–10000	1.00	[47]
Ru[(tpy)(bpy)Cl]PF6/sol-gel CCE	5.00–685	1.00	[48]
MWCNTs-modified GCE	10.0–500	5.40	[49]
Au-SH-SiO ₂ @Cu-MOF	0.02–300	0.008	[25]
Poly-3,4-hylenedioxythiophene/screen-printed electrode	0.05–200	0.03	[50]
Copper-cobalt hexacyanoferrate/ CPE	6.00–1000	5.00	[51]
This work	1–11.0	0.04	

CPE carbon paste electrode, GCE glassy carbon electrode, CCE carbon ceramic electrode, MOF metal-organic framework

electrodepositing of ACA on the surface of PNA/ZnSe-QD AuNP Au electrode. Compared with Au/AuNPs/ACA, Au/PNA/ZnSe-QD/ACA and Au/ACA, combination of ZnSe-QD and AuNPs resulted in improvement of both the reversibility and current responses of Au/AuNPs/PNA/ZnSe-QD/ACA electrode. The Au/AuNPs/PNA/ZnSe-QD/ACA electrode also enhanced electrocatalytic activity toward oxidation of CySH. It was also found that the peak potential for oxidation of CySH was significantly shifted to a more negative potential (0.05 V vs. Ag/AgCl) compared to that of the Au/AuNPs/PNA/ZnSe-QD modified electrode (0.55 V vs. Ag/AgCl). Some kinetic parameters, such as the electron transfer coefficient, the diffusion coefficient of CySH and the catalytic rate constant k_{cat} of the catalytic reaction were calculated. A sensitive amperometric method was proposed for determination of CySH with the advantages of fast response and good reproducibility.

Acknowledgments The authors gratefully acknowledge the support of this work by the Khorramabad Branch, Islamic Azad University for financial support.

Open Access This article is distributed under the terms of the Creative Commons Attribution License which permits any use, distribution, and reproduction in any medium, provided the original author(s) and the source are credited.

References

- J.C. Claussen, A.D. Franklin, A. Haque, D.M. Porterfield, T.S. Fisher, Electrochemical biosensor of nanocube-augmented carbon nanotube networks. *ACS Nano* **3**(1), 37–44 (2009). doi:10.1021/nn800682m
- T.G. Drummond, M.G. Hill, J.K. Barton, Electrochemical DNA sensors. *Nat. Biotechnol.* **21**(10), 1192–1199 (2003). doi:10.1038/nbt873
- F. Patolsky, G. Zheng, C.M. Lieber, Nanowire sensors for medicine and the life sciences. *Nanomedicine* **1**(1), 51–65 (2006). doi:10.2217/17435889.1.1.51
- M. Hung, D.M. Stanbury, Catalytic and direct oxidation of cysteine by octacyanomolybdate(V). *Inorg. Chem.* **44**(10), 3541–3550 (2005). doi:10.1021/ic050427c
- T. Inoue, J.R. Kirchhoff, Electrochemical detection of thiols with a coenzyme pyrroloquinoline quinone modified electrode. *Anal. Chem.* **72**(23), 5755–5760 (2000). doi:10.1021/ac000716c
- M.M. Ardakani, P. Rahimi, P.E. Karami, H.R. Zare, H. Naeimi, Electrocatalytic oxidation of cysteine by quinizarine at glassy carbon electrode. *Sens. Actuators B* **123**(2), 763–768 (2007). doi:10.1016/j.snb.2006.10.015
- S. Shahrokhian, Lead phthalocyanine as a selective carrier for preparation of a cysteine-selective electrode. *Anal. Chem.* **73**(24), 5972–5978 (2001). doi:10.1021/ac010541m
- P.C. White, N.S. Lawrence, J. Davis, R.G. Compton, Electrochemically initiated 1, 4 additions: a versatile route to the determination of thiols. *Anal. Chim. Acta* **447**(1–2), 1–10 (2001). doi:10.1016/S0003-2670(01)01297-1
- S. Seshadri, A. Beiser, J. Selhub, P.F. Jacques, I.H. Rosenberg, R.B. D’Agostino, P.W.F.N. Wilson, P.A. Wolf, Plasma homocysteine as a risk factor for dementia and alzheimer’s disease. *N. Engl. J. Med.* **346**(7), 476–483 (2002). doi:10.1056/NEJMoa011613
- M.A. Hofmann, B. Kohl, M.S. Zumbach, V. Borcea, A. Bierhaus, M. Henkels, J. Amiral, W. Fiehn, R. Ziegler, P. Wahl, P.P. Nawroth, Hyperhomocyst(e)inemia and endothelial dysfunction in IDDM. *Diabetes Care* **20**(12), 1880–1886 (1997). doi:10.2337/diacare.20.12.1880
- E.K. Hoogeveen, P.J. Kostense, P.J. Beks, A.J.C. Mackaay, C. Jakobs, L.M. Bouter, R.J. Heine, C.D. Stehouwer, Hyper homocysteinemia is associated with an increased risk of cardiovascular disease, especially in non-insulin dependent diabetes mellitus: a population-based study. *Arterioscler. Thromb. Vasc. Biol.* **18**(1), 133–138 (1998). doi:10.1161/01.ATV.18.1.133
- B. Hultberg, E. Agardh, A. Andersson, L. Brattstrom, A. Isaksson, B. Israelsson, C.D. Agardh, Increased levels of plasma homocysteine are associated with nephropathy, but not severe retinopathy in type 1 diabetes mellitus. *Scand. J. Clin. Lab. Inv.* **51**(3), 277–282 (1991). doi:10.3109/00365519109091615
- E. Sharifi, A. Salimi, E. Shams, DNA/nickel oxide nanoparticles/osmium(III)-complex modified electrode toward selective oxidation of L-cysteine and simultaneous detection of L-cysteine and homocysteine. *Bioelectrochemistry* **86**(6), 9–21 (2012). doi:10.1016/j.bioelechem.2011.12.013
- W. Wang, O. Rusin, X. Xu, K.K. Kim, J.O. Escobedo, S.O. Fakayode, K.A. Fletcher, M. Lowry, C.M. Schowalter, C.M. Lawrence, F.R. Fronczek, I.M. Warner, R.M. Strongin, Detection of homocysteine and cysteine. *J. Am. Chem. Soc.* **127**(45), 15949–15958 (2005)
- G. Chwatko, E. Bald, Determination of cysteine in human plasma by high-performance liquid chromatography and ultraviolet detection after pre-column derivatization with 2-chloro-1-methylpyridinium iodide. *Talanta* **52**(3), 509–515 (2000). doi:10.1016/S0039-9140(00)00394-5
- A. Sano, H. Nakamura, Chemiluminescence detection of thiols by high-performance liquid chromatography using o-Phthalaldehyde and N-(4-Aminobutyl)-N-ethylisoluminol as precolumn derivatization reagents. *Anal. Sci.* **14**(4), 731–737 (1998). doi:10.2116/analsci.14.731
- K. Arlt, S. Brandt, J. Kehr, Amino acid analysis in five pooled single plant cell samples using capillary electrophoresis coupled to laser-induced fluorescence detection. *J. Chromatogr. A* **926**(2), 319–325 (2001). doi:10.1016/S0021-9673(01)01052-4
- M. Ummadi, B.C. Weimer, Use of capillary electrophoresis and laser-induced fluorescence for attomole detection of amino acids. *J. Chromatogr. A* **964**(1–2), 243–253 (2002). doi:10.1016/S0021-9673(02)00692-1
- F. Tanaka, N. Mase, C.F. Barbas, Determination of cysteine concentration by fluorescence increase: reaction of cysteine with a fluorogenic aldehyde. *Chem. Commun.* **5**, 1762–1763 (2004). doi:10.1039/b405642f
- D.A.M. Zaia, K.C.L. Ribas, C.T.B.V. Zaia, Spectrophotometric determination of cysteine and/or carbocysteine in a mixture of amino acids, shampoo, and pharmaceutical products using p-benzoquinone. *Talanta* **50**(5), 1003–1010 (1999). doi:10.1016/S0039-9140(99)00218-0
- G. Shi, J. Lu, F. Xu, W. Sun, L. Jin, K. Yamamoto, S. Tao, J. Jin, Determination of glutathione in vivo by microdialysis using liquid chromatography with a cobalt hexacyanoferrate chemically modified electrode. *Anal. Chim. Acta* **391**(4), 307–313 (1999). doi:10.1016/S0003-2670(99)00274-3
- F. Pak, K. Meral, R. Altundaş, D. Ekinci, Self-assembled monolayers of fluorene- and nitrofluorene-terminated thiols on polycrystalline gold electrode: electrochemical and optical properties. *J. Electroanal. Chem.* **654**(1–2), 20–28 (2011). doi:10.1016/j.jelechem.2011.01.041
- S.M. Chen, J.Y. Chen, R. Thangamuthu, Electrochemical preparation of brilliant-blue-modified poly(diallyldimethylammoniumchloride) and nafion-coated glassy carbon electrodes and their electrocatalytic

- behavior towards oxygen and L-cysteine. *Electroanalysis* **20**(14), 1565–1573 (2008). doi:[10.1002/elan.200804213](https://doi.org/10.1002/elan.200804213)
24. S. Ge, M. Yan, J. Lu, M. Zhang, F. Yu, J. Yu, X. Song, S. Yu, Electrochemical biosensor based on graphene oxide–Au nanoclusters composites for L-cysteine analysis. *Biosens. Bioelectron.* **31**(1), 49–54 (2012). doi:[10.1016/j.bios.2011.09.038](https://doi.org/10.1016/j.bios.2011.09.038)
 25. H. Hosseini, H. Ahmar, A. Dehghani, A. Bagheri, A. Tadjarodi, A.R. Fakhari, A novel electrochemical sensor based on metal-organic framework for electro-catalytic oxidation of L-cysteine. *Biosens. Bioelectron.* **42**, 426–429 (2013). doi:[10.1016/j.bios.2012.09.062](https://doi.org/10.1016/j.bios.2012.09.062)
 26. M. Zhou, J. Ding, L.-P. Guo, Q.-K. Shang, Electrochemical behavior of L-cysteine and its detection at ordered mesoporous-carbon-modified glassy carbon electrode. *Anal. Chem.* **79**(14), 5328–5335 (2007). doi:[10.1021/ac0703707](https://doi.org/10.1021/ac0703707)
 27. M. Liu, G. Shi, L. Zhang, Y. Cheng, L. Jin, Quantum dots modified electrode and its application in electroanalysis of hemoglobin. *Electrochem. Commun.* **8**(2), 305–310 (2006). doi:[10.1016/j.elecom.2005.11.026](https://doi.org/10.1016/j.elecom.2005.11.026)
 28. J. Drbohlavova, V. Adam, R. Kizek, J. Hubalek, Quantum dots-characterization, preparation and usage in biological systems. *Int. J. Mol. Sci.* **10**(2), 656–673 (2009). doi:[10.3390/ijms10020656](https://doi.org/10.3390/ijms10020656)
 29. J. Aldana, Y.A. Wang, X. Peng, Photochemical instability of CdSe nanocrystals coated by hydrophilic thiols. *J. Am. Chem. Soc.* **123**(36), 8844–8850 (2001). doi:[10.1021/ja016424q](https://doi.org/10.1021/ja016424q)
 30. M.J. Giz, B. Duong, N.J. Tao, In situ STM study of self-assembled mercaptopropionic acid monolayers for electrochemical detection of dopamine. *J. Electroanal. Chem.* **465**(1), 72–79 (1999). doi:[10.1016/S0022-0728\(99\)00056-X](https://doi.org/10.1016/S0022-0728(99)00056-X)
 31. J. Li, G. Zou, X. Hu, X. Zhang, Electrochemistry of thiol-capped CdTe quantum dots and its sensing application. *J. Electroanal. Chem.* **625**(1), 88–91 (2009). doi:[10.1016/j.jelechem.2008.10.011](https://doi.org/10.1016/j.jelechem.2008.10.011)
 32. J. Berna, M. Alajarín, R.A. Orenes, Azodicarboxamides as template binding motifs for the building of hydrogen-bonded molecular shuttles. *J. Am. Chem. Soc.* **132**(31), 10741–10747 (2010). doi:[10.1021/ja101151t](https://doi.org/10.1021/ja101151t)
 33. H. Cui, Y. Xu, Z.F. Zhang, Multichannel electrochemiluminescence of luminol in neutral and alkaline aqueous solutions on a gold nanoparticle self-assembled electrode. *Anal. Chem.* **76**(14), 4002–4010 (2004). doi:[10.1021/ac049889i](https://doi.org/10.1021/ac049889i)
 34. J.J. Andrade, J.A. Brasil Jr, P.M.A. Farias, A. Fontes, B.S. Santos, Synthesis and characterization of blue emitting ZnSe quantum dots. *Microelectron. J.* **40**(3), 641–643 (2009). doi:[10.1016/j.mejo.2008.06.040](https://doi.org/10.1016/j.mejo.2008.06.040)
 35. V. Swayambunathan, D. Hayes, K.H. Schmidt, Y.X. Liao, D. Meisel, Thiol surface complexation on growing cadmium sulfide clusters. *J. Am. Chem. Soc.* **112**(10), 3831–3837 (1990). doi:[10.1021/ja00166a017](https://doi.org/10.1021/ja00166a017)
 36. M.B. Gholivand, A. Azadbakht, Fabrication of a highly sensitive glucose electrochemical sensor based on immobilization of Ni(II)–pyromellitic acid and bimetallic Au–Pt inorganic–organic hybrid nanocomposite onto carbon nanotube modified glassy carbon electrode. *Electrochim. Acta* **76**, 300–311 (2012). doi:[10.1016/j.electacta.2012.05.037](https://doi.org/10.1016/j.electacta.2012.05.037)
 37. S. Antoniadou, A.D. Jannakoudakis, E. Theodoridou, Electrocatalytic reactions on carbon fibre electrodes modified by hemine II. Electro-oxidation of hydrazine. *Synth. Met.* **30**(3), 295–304 (1980). doi:[10.1016/0379-6779\(89\)90652-8](https://doi.org/10.1016/0379-6779(89)90652-8)
 38. E. Laviron, General expression of the linear potential sweep voltammogram in the case of diffusionless electrochemical systems. *J. Electroanal. Chem.* **101**(1), 19–28 (1979). doi:[10.1016/S0022-0728\(79\)80075-3](https://doi.org/10.1016/S0022-0728(79)80075-3)
 39. A.J. Bard, L.R. Faulkner, *Electrochemical Methods: Fundamentals and Applications*, 2nd edn. (Wiley, New York, 2000)
 40. J.A. Harrison, Z.A. Khan, The oxidation of hydrazine on platinum in acid solution. *J. Electroanal. Chem.* **28**(1), 131–138 (1970). doi:[10.1016/S0022-0728\(70\)80288-1](https://doi.org/10.1016/S0022-0728(70)80288-1)
 41. T.R. Ralph, M.L. Hitchman, J.P. Millington, F.C. Walsh, The electrochemistry of L-cystine and L-cysteine: part 1: Thermodynamic and kinetic studies. *J. Electroanal. Chem.* **375**(1–2), 1–15 (1994). doi:[10.1016/0022-0728\(94\)03407-9](https://doi.org/10.1016/0022-0728(94)03407-9)
 42. Z. Galus, *Fundamentals of Electrochemical Analysis* (Horwood, New York, 1976)
 43. X. Tang, Y. Liu, H. Hou, T. You, Electrochemical determination of L-Tryptophan, L-Tyrosine and L-Cysteine using electrospun carbon nanofibers modified electrode. *Talanta* **80**(5), 2182–2186 (2010). doi:[10.1016/j.talanta.2009.11.027](https://doi.org/10.1016/j.talanta.2009.11.027)
 44. R. Ojani, J.B. Raoof, E. Zarei, Preparation of poly *N, N*-dimethylaniline/ferrocyanide film modified carbon paste electrode: application to electrocatalytic oxidation of L-cysteine. *J. Electroanal. Chem.* **638**(2), 241–245 (2010). doi:[10.1016/j.jelechem.2009.11.005](https://doi.org/10.1016/j.jelechem.2009.11.005)
 45. J.C. Ndamanisha, J. Bai, B. Qi, L. Guo, Application of electrochemical properties of ordered mesoporous carbon to the determination of glutathione and cysteine. *Anal. Biochem.* **386**(1), 79–84 (2009). doi:[10.1016/j.ab.2008.11.041](https://doi.org/10.1016/j.ab.2008.11.041)
 46. J.M. Zen, A.S. Kumar, J.-C. Chen, Electrocatalytic oxidation and sensitive detection of cysteine on a lead ruthenate pyrochlore modified electrode. *Anal. Chem.* **73**(6), 1169–1175 (2001). doi:[10.1021/ac0010781](https://doi.org/10.1021/ac0010781)
 47. M.K. Amini, J.H. Khorasani, S.S. Khaloo, S. Tangestaninejad, Cobalt(II) salophen-modified carbon-paste electrode for potentiometric and voltammetric determination of cysteine. *Anal. Biochem.* **320**(1), 32–38 (2003). doi:[10.1016/S0003-2697\(03\)00355-5](https://doi.org/10.1016/S0003-2697(03)00355-5)
 48. A. Salimi, S. Pourbeyram, Renewable sol–gel carbon ceramic electrodes modified with a Ru-complex for the amperometric detection of L-cysteine and glutathione. *Talanta* **60**(1), 205–214 (2003). doi:[10.1016/S0039-9140\(03\)00125-5](https://doi.org/10.1016/S0039-9140(03)00125-5)
 49. A. Salimi, R. Hallaj, Catalytic oxidation of thiols at preheated glassy carbon electrode modified with abrasive immobilization of multiwall carbon nanotubes: applications to amperometric detection of thiocytosine, L-cysteine and glutathione. *Talanta* **66**(4), 967–975 (2005). doi:[10.1016/j.talanta.2004.12.040](https://doi.org/10.1016/j.talanta.2004.12.040)
 50. W.Y. Su, S.H. Cheng, Electrocatalysis and sensitive determination of cysteine at poly(3,4-ethylenedioxythiophene)-modified screen-printed electrodes. *Electrochem. Commun.* **10**(6), 899–902 (2008). doi:[10.1016/j.elecom.2008.04.013](https://doi.org/10.1016/j.elecom.2008.04.013)
 51. A. Abbaspour, A. Ghaffarinejad, Electrocatalytic oxidation of L-cysteine with a stable copper–cobalt hexacyanoferrate electrochemically modified carbon paste electrode. *Electrochim. Acta* **53**(22), 6643–6650 (2008). doi:[10.1016/j.electacta.2008.04.065](https://doi.org/10.1016/j.electacta.2008.04.065)
 52. Y.P. Dong, L. Pei, X.F. Chu, W.B. Zhang, Q.F. Zhang, Electrochemical behavior of cysteine at a CuGeO₃ nanowires modified glassy carbon electrode. *Electrochim. Acta* **55**(18), 5135–5141 (2010). doi:[10.1016/j.electacta.2010.04.020](https://doi.org/10.1016/j.electacta.2010.04.020)
 53. P. Sweth, A.S. Kumar, Phosphomolybdic acid nano-aggregates immobilized nafion membrane modified electrode for selective cysteine electrocatalytic oxidation and anti-dermatophytic activity. *Electrochim. Acta* **98**, 54–65 (2013). doi:[10.1016/j.electacta.2013.03.023](https://doi.org/10.1016/j.electacta.2013.03.023)
 54. H. Razmi, A. Azadbakht, Electrochemical characteristics of dopamine oxidation at palladium hexacyanoferrate film, electrodeless plated on aluminum electrode. *Electrochim. Acta* **50**(11), 2193–2201 (2005). doi:[10.1016/j.electacta.2004.10.001](https://doi.org/10.1016/j.electacta.2004.10.001)
 55. A.A. Ensafi, S. Behyan, Sensing of L-cysteine at glassy carbon electrode using Nile blue A as a mediator. *Sens. Actuators B* **122**(1), 282–288 (2007). doi:[10.1016/j.snb.2006.05.035](https://doi.org/10.1016/j.snb.2006.05.035)
 56. S.P. Stabler, P.D. Marcell, E.R. Podell, R.H. Allen, Quantitation of total homocysteine, total cysteine, and methionine in normal serum and urine using capillary gas chromatography-mass spectrometry. *Anal. Biochem.* **162**(1), 185–196 (1987). doi:[10.1016/0003-2697\(87\)90026-1](https://doi.org/10.1016/0003-2697(87)90026-1)